remote sensing

MDPI

Article

Disentangling the Effects of Atmospheric and Soil Dryness on Autumn Phenology across the Northern Hemisphere

Kangbo Dong [1,2] and Xiaoyue Wang [1,2,*]

[1] The Key Laboratory of Land Surface Pattern and Simulation, Institute of Geographic Sciences and Natural Resources Research, Chinese Academy of Sciences, Beijing 100101, China; dongkangbo22@mails.ucas.ac.cn
[2] University of Chinese Academy of Sciences, Beijing 100049, China
* Correspondence: wangxy@igsnrr.ac.cn

Abstract: In recent decades, drought has intensified along with continuous global warming, significantly impacting terrestrial vegetation. High atmospheric water demand, indicated by vapor pressure deficit (VPD), and insufficient soil moisture (SM) are considered the primary factors causing drought stress in vegetation. However, the influences of VPD and SM on the autumn phenology are still unknown. Using satellite observations and meteorological data, we examined the impacts of VPD and SM on the end of the growing season (EOS) across the Northern Hemisphere (>30°N) from 1982 to 2022. We found that VPD and SM were as important as temperature, precipitation, and radiation in controlling the variations in the EOS. Moreover, the EOS was predominantly influenced by VPD or SM in more than one-third (33.8%) of the study area. In particular, a ridge regression analysis indicated that the EOS was more sensitive to VPD than to SM and the other climatic factors, with 25% of the pixels showing the highest sensitivity to VPD. In addition, the effects of VPD and SM on the EOS varied among biome types and climate zones. VPD significantly advanced the EOS in 25.8% of temperate grasslands, while SM had the greatest impact on advancing the EOS in 17.7% of temperate coniferous forests. Additionally, 27.7% of the midlatitude steppe (BSk) exhibited a significant negative correlation between VPD and the EOS, while 19.4% of the marine west coast climate (Cfb) showed a positive correlation between SM and the EOS. We also demonstrated that the correlation between VPD and the EOS was linearly affected by VPD and the leaf area index, while the correlation between SM and the EOS was affected by SM, precipitation, and the leaf area index. Our study highlights the importance of VPD and SM in regulating autumn phenology and enhances our understanding of terrestrial ecosystem responses to climate change.

Keywords: autumn vegetation phenology; drought; vapor pressure deficit; soil moisture

Citation: Dong, K.; Wang, X. Disentangling the Effects of Atmospheric and Soil Dryness on Autumn Phenology across the Northern Hemisphere. *Remote Sens.* **2024**, *16*, 3552. https://doi.org/10.3390/rs16193552

Academic Editor: Brenden E. McNeil

Received: 27 August 2024
Revised: 18 September 2024
Accepted: 19 September 2024
Published: 24 September 2024

1. Introduction

Terrestrial vegetation, as a crucial element of terrestrial ecosystems, is highly significant in adjusting the exchange of water, carbon, and energy between the atmosphere and the land surface, thereby stabilizing atmospheric carbon dioxide and mitigating climate warming [1]. Vegetation phenology, defined as the timing of cyclical features in plant growth and their duration [2,3], e.g., the start (SOS) and end (EOS) of the growing season, serves as a direct index of climate change [2,4]. There is ample research showing that the EOS is vital in vegetation growth and in regulating the carbon sink and terrestrial water cycles [5,6], but this has been largely neglected [7].

Limited water availability affects terrestrial vegetation productivity in many regions [8] and has become a recurring condition that negatively impacts vegetation growth and phenology, particularly in Mediterranean, arid, and semi-arid ecosystems [9]. Climate change has led to progressively more drought events, which are among the most impactful natural disasters affecting ecological and human systems [10] and have a non-negligible role in vegetation phenology, growth, and survival [11].

High vapor pressure deficit (VPD), reflecting atmospheric water demand, and low soil moisture (SM) supply are considered the two primary drivers of drought stress on vegetation, posing significant threats to agricultural production and causing widespread vegetation mortality [12,13]. SM provides water directly to vegetation and is more vulnerable to droughts, affecting autumn vegetation phenology [14]. VPD, defined as the difference between the saturated vapor pressure and actual vapor pressure, could significantly influence stomatal conductance and photosynthesis [15,16]. The stomata of vegetation close to reduce exorbitant water loss with a high VPD, which causes a reduction in photosynthesis and carbon uptake by the vegetation [15,17,18]. There is research showing that an increase in VPD significantly affects vegetation productivity [16,19], forest mortality [20], and the global terrestrial carbon sink [21], while studies have shown that VPD is an important determinant of water resources and vegetation–water relationships [19].

However, discussions are ongoing on the roles of soil moisture and vapor pressure deficits in deciding the effects of droughts on vegetation, leading to different conclusions regarding drought stress on vegetation [22]. On the one hand, SM supplies water directly to the vegetation, determining the amount of water that is extractable by the roots [22], making low SM a common indicator of vegetation drought stress and the impact on productivity [23,24]. On the other hand, a high VPD induces stomatal closure to minimize water damage [25] and constrains photosynthesis. Several studies have expressed the importance of VPD and suggested that it might affect vegetation more than SM [15,16,19,26]. However, another study has shown that soil moisture dominates drought stress on vegetation [27]. It has been shown that VPD changes are influenced by air moisture content and temperature [15], while SM significantly impacts evapotranspiration [28]. During a drought, low SM limits evapotranspiration, potentially affecting VPD [28]. Increased foliage cover in the Northern Hemisphere can further deplete soil moisture, leading to a higher VPD [29]. Strong negative coupling between VPD and SM globally indicates a high probability of concurrent atmospheric aridity and soil dryness, aggravated by land–atmosphere feedback [30]. To date, the respective influences of VPD and SM on vegetation, particularly on autumn phenology, remain debated and challenging to disentangle. Identifying these effects is vital for researching the responses of terrestrial vegetation to climate change and predicting future changes in the ecosystem carbon cycle. In this study, with satellite observations of the EOS and a climate dataset, the strong correlations of VPD and SM with the EOS were explored, and their respective effects were discerned.

2. Data and Methods

2.1. Study Area

Our study focused on natural vegetation in the Northern Hemisphere (>30°N), where vegetation dynamics show evident seasonality, facilitating the extraction of the EOS [31]. This wider study area was classified into seven types based on the biome categories from Terrestrial Ecoregions of the World (Figure 1a) [32]. Cultivation areas were eliminated due to the interference of human activities, using the MODIS Land Cover Type Product (MCD12Q1) [33].

Simultaneously, the wider study area was classified into seven climate zones according to the Köppen–Geiger climate zone classification, one of the most widely used classifications of climate zones in studies for its accuracy and universality and its simple access and process; the categories in the study area included midlatitude steppe (BSk), marine west coast climate (Cfb), humid continental climate (Dfb), subarctic climate (Dfd), another type of subarctic climate (Dwc), and tundra (ET) (Figure 1b).

Focusing on the regions with evident phenology, the only pixels included were those indicating that the July and August NDVI was more than 1.2 times the mean NDVI of winter, the EOS occurred after June, and the annual maximum NDVI appeared between June and October [34,35].

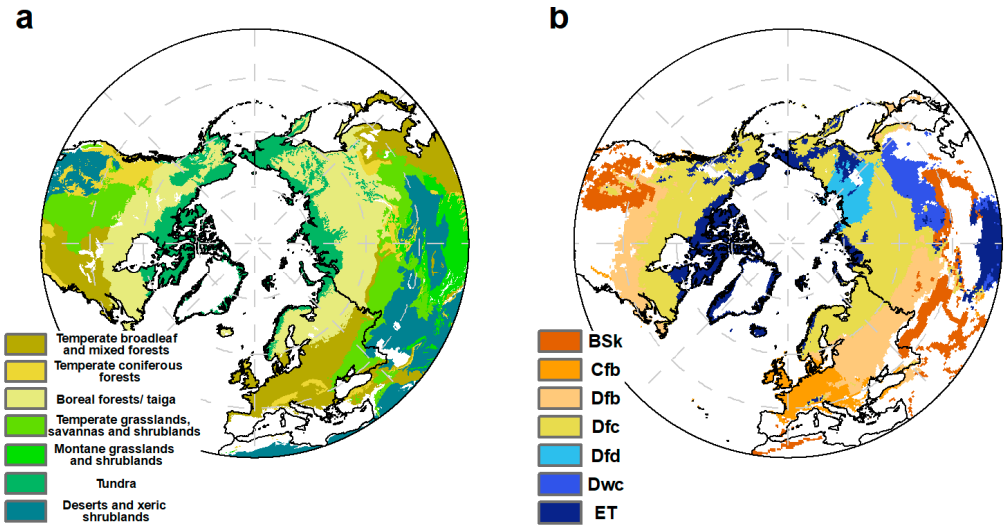

Figure 1. (**a**) Biome type (*Terrestrial Ecoregions of the World*) (>30°N). (**b**) Köppen–Geiger climate zones (>30°N).

2.2. Data

2.2.1. EOS and LAI from GIMMS Data

GIMMS3g+, an enhanced third-generation long-term GIMMS AVHRR dataset (https://daac.ornl.gov/VEGETATION/guides/Global_Veg_Greenness_GIMMS_3G.html, accessed on 10 September 2023) was published by the National Aeronautics and Space Administration (NASA). The dataset includes the leaf area index (LAI) and normalized differential vegetation index (NDVI), adopting the WGS84 world geodetic coordinate system with a 15-day temporal resolution and a 0.0833° spatial resolution [36]; it has become one of the most widely used datasets for studying and simulating vegetation [37]. Based on the QC quality index of GIMMS3g+ data, low-quality observation data such as snow cover and cloud fog were identified, and low weights were assigned to the data during the fitting to avoid the interference of outliers. We then used a curve fitting method [38] to obtain the daily NDVI curve and reduce the impact of outliers.

The EOS was obtained through the daily NDVI curve, and the EOS was determined as the day of the year when the $NDVI_{ratio}$ decreased to 0.5 for the respective pixel (Figure 2). The $NDVI_{ratio}$ was defined as follows:

$$NDVI_{ratio} = \frac{NDVI - NDVI_{min}}{NDVI_{max} - NDVI_{min}} \quad (1)$$

where $NDVI_{ratio}$ is the ratio of NDVI, ranging from 0 to 1. $NDVI_{min}$ and $NDVI_{max}$ represent the minimum value and maximum value of the smoothed NDVI curve, respectively.

2.2.2. Meteorological and Other Supporting Data

The VPD and SM data were obtained from the Terraclimate dataset (https://gee-community-catalog.org/projects/terraclim/, accessed on 15 September 2023). The drought datasets were averaged by month at a spatial resolution of 4 km (1/24°) from 1958 to 2022 [39].

Three other factors, namely, mean temperature (TMEAN), precipitation (PPT), and solar radiation (SRAD), were used to account for the response of the EOS to drought, obtained from the Terraclimate dataset [39].

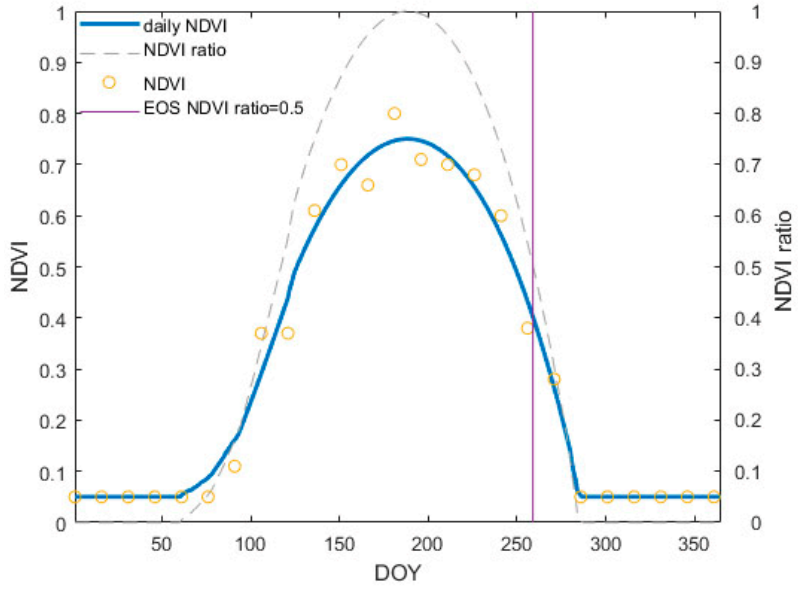

Figure 2. An illustration of the method used to extract the end of the growing season (EOS) from NDVI data.

2.3. Methods

2.3.1. Partial Correlation Analysis

Meteorological forces generally affect vegetation for a few months before the EOS. The preseason lengths of factors are different due to vegetation types and positions, and the most appropriate preseason length was determined using partial correlation coefficients between the EOS and VPD or SM with a time span ranging from June to the month containing the EOS, controlling other corresponding factors. It was determined that the time span whose absolute partial correlation coefficient was the highest should be the correct preseason length at the respective pixels [40].

The correlations of the EOS with preseason VPD/SM and other factors were determined through a partial correlation analysis. To analyze the influences of dryness on the EOS, we used other variables as controlling factors in the partial correlation analyses. The values of the coefficients indicate the relative importance and show which climate factors affect the EOS more. We first standardized all the variables and then calculated the partial correlation coefficients in each pixel of the study area, presenting the contributions of individual factors to the EOS without the influences of other factors.

2.3.2. Ridge Regression

A ridge regression analysis was applied to assess the sensitivities of EOS to VPD, SM, and other climate factors, reducing the effects of multicollinearity on the correct detection [41]; this linear regularization method could effectively eliminate multicollinearity and is thus appropriate for an analysis among independent variables with severe multicollinearity. We employed normalized anomalies of VPD, SM, other climate factors, and the EOS as inputs for the regression analysis, with the resulting regression coefficients representing the sensitivities of each factor. To facilitate a direct comparison of the effects of different factors on the EOS, we calculated the absolute values of the regression coefficients. For each pixel, the factor associated with the highest absolute coefficient was identified as the most influential on the EOS.

2.3.3. Decoupling the Relative Effects of VPD and SM on the EOS

VPD and SM were typically strongly coupled in both their temporal and spatial distributions, leading to ambiguity in determining their individual effects on EOS. To disentangle these effects, we first calculated threshold values corresponding to the 10th, 20th, . . ., and 90th percentiles of the sorted VPD and SM for each pixel in the study area,

which were then used to categorize the EOS values into bins. The VPD and SM data were divided into 10 bins based on the aforementioned thresholds, representing the 0–10th, 10–20th, . . ., 80–90th, and 90–100th percentiles of VPD or SM [22,42,43]. Subsequently, the EOS values within each SM bin were sorted based on VPD thresholds, and vice versa, resulting in a total of 100 bins (10 bins for VPD and 10 bins for SM). We then computed the mean EOS for the pixels corresponding to each of these bins, yielding 100 average EOS values across the different percentiles of VPD and SM. This approach allowed us to independently assess the changes in EOS with respect to VPD or SM, without interference from the other variable.

3. Results

3.1. Spatial and Temporal Patterns of EOS, SM, and VPD

The spatial distribution of the averaged EOS from 1982 to 2022 is presented in Figure 3a. EOS mainly occurred between day of year (DOY) 240 and DOY 260, accounting for about 80% of the study area. The standard deviation was mostly between 5 and 15 days, accounting for about 82% (Figure 3b). The EOS slope from 1982 to 2022 was mostly between −0.2 and 0.4 day/year, accounting for 63%, and about 57% of the entire study area presented a positive slope (Figure 3c). Within the study area, 36% of the pixels exhibited a significant trend ($p < 0.05$) (Figure 3d).

Regarding the averaged SM from 1982 to 2022, we found that it primarily ranged from 10 to 50 mm, accounting for about 60% (Figure 3e), and the lowest SM was found in East Asia (Figure 3e), while the standard deviation of SM from 1982 to 2022 was mostly distributed from 0 to 12 mm, accounting for about 80% (Figure 3f). In addition, the SM slope from 1982 to 2022 was mostly between −0.2 and 0.2 mm/year, accounting for about 77%, and about 46% of the whole study area presented a positive slope (Figure 3g). Within the study area, 20% of the pixels exhibited a significant trend ($p < 0.05$) (Figure 3h).

We found that the averaged VPD from 1982 to 2022 was mainly distributed from 0.1 to 0.4, accounting for about 81% (Figure 3i). The lowest VPD mainly appeared in Northern Canada and northern Russia, and the highest VPD mainly appeared in East Asia and the central areas of the United States (Figure 3i). We found that the standard deviation of VPD from 1982 to 2022 was mostly distributed from 0.01 to 0.04, accounting for about 76% (Figure 3j). In addition, the slope of VPD from 1982 to 2022 was mostly distributed from 0 to 0.002/year, accounting for about 77%, and about 91% of the total study area presented a positive slope (Figure 3k). In the study area, 56% of the pixels exhibited a significant trend ($p < 0.05$) (Figure 3l).

3.2. The Effects of VPD and SM on the EOS

We found that the EOS was significantly correlated with SM for 19.3% and VPD for 18.1% of all pixels ($p < 0.05$), among which 73.06% showed positive correlations between the EOS and SM and 68.5% expressed negative correlations between the EOS and VPD. SM played the most important role in 18.4% of the study area, and VPD in 15.4% (Figure 4). About 59% of the values of the correlation coefficients between the EOS and VPD were from −0.6 to −0.1, and about 35% of these were from 0.1 to 0.4. Regarding the values of the correlation coefficients between the EOS and SM, about 39% were from −0.6 to 0.1, and about 56% were from 0.1 to 0.5; for PPT, about 52% were from −0.6 to 0.1 and 44% from 0.1 to 0.5; for SRAD, about 34% were from −0.5 to −0.1 and about 62% from 0.1 to 0.5; and for Tmean, about 38% were from −0.5 to −0.1 and 56% from 0.1 to 0.5.

In most areas of North America and Central Asia, the number of pixels in which the EOS was negatively significantly correlated with VPD was obviously higher than the number of pixels in which the EOS exhibited significantly positive correlations with VPD. Inversely, the number of pixels in which the EOS exhibited significantly positive correlations with VPD was obviously higher than the number of pixels in which the EOS exhibited significantly negative correlations with VPD in most areas of Northern Europe. In most areas east of the Ural Mountains, the number of pixels in which the EOS was negatively sig-

nificantly correlated with SM was obviously higher than the number of pixels in which the EOS exhibited significantly positive correlations with SM. Inversely, the number of pixels in which the EOS exhibited significantly positive correlations with SM was obviously higher than the number of pixels in which the EOS exhibited significantly negative correlations with SM in most areas of Northern Europe, Central Asia, and North America.

Using the ridge regression analysis of the data from 1982 to 2022, representing the sensitivity of EOS to VPD and SM, a contrast in the independent influences of SM and VPD on EOS was found. We found that the EOS exhibited positive correlations with VPD in 57.7% of the study area and negative correlations in 42.4% of the study area, and the EOS was positively correlated with SM in 62% of the study area and negatively correlated in 38%. SM played the most important role in 10.2% of the study area, and VPD in 25% (Figure 5). In most areas of Central Asia and North America, the EOS was negatively correlated with VPD. Inversely, the EOS exhibited positive correlations with VPD in most areas in the west of Russia and the north of West Siberia. In most areas of Northern Europe, North America, and Asia, the EOS was positively correlated with SM. We found that the sensitivity of the EOS to VPD was obviously higher than to other factors, while the coefficients of partial correlation between the EOS and VPD were almost equal to the others.

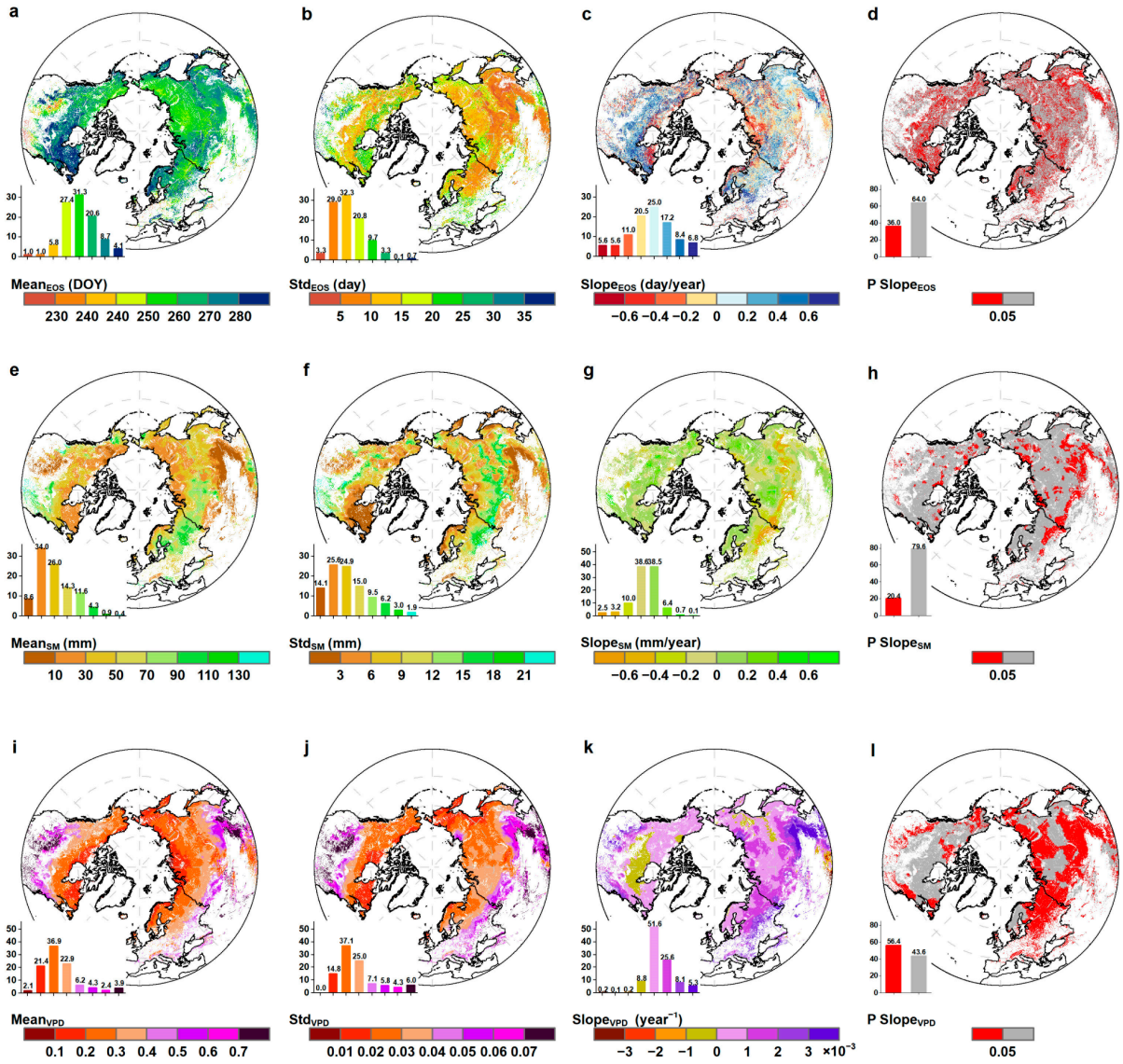

Figure 3. Spatial distributions of the mean (**a**,**e**,**i**), standard deviation (**b**,**f**,**j**), slope (**c**,**g**,**k**), and significance level (**d**,**h**,**l**) of the EOS, SM, and VPD from 1982 to 2022, respectively.

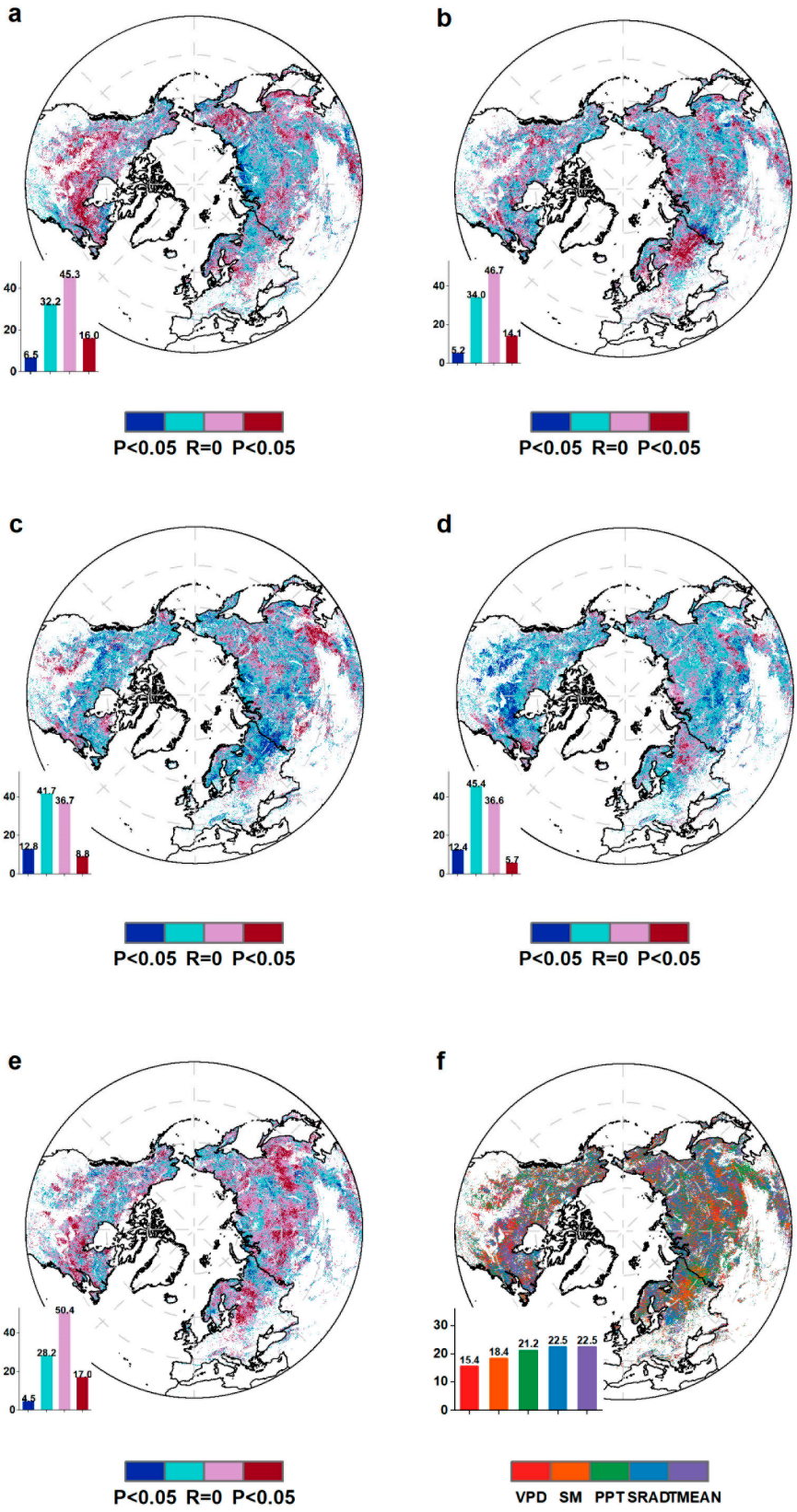

Figure 4. Spatial pattern of partial correlation coefficients between factors and EOS: (**a**) averaged temperature, (**b**) soil moisture, (**c**) precipitation, (**d**) vapor pressure deficit, (**e**) solar radiation, and (**f**) the most dominant factor. The gray areas represent non-significant pixels. The bars on the left express the proportions of the partial correlation coefficients between the EOS and corresponding factors.

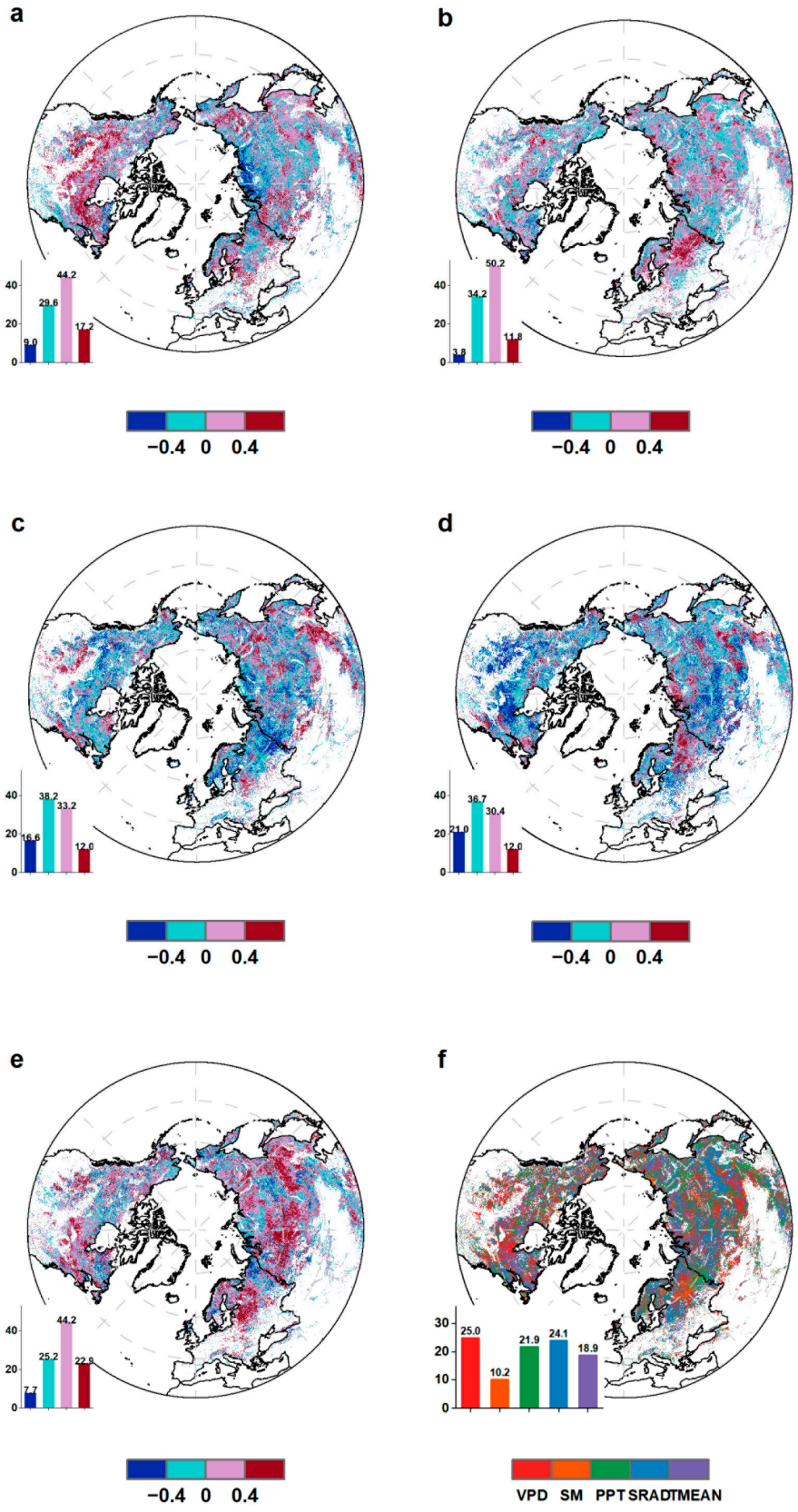

Figure 5. Spatial pattern of ridge regression coefficients between climatic factors and the EOS: (**a**) averaged temperature, (**b**) soil moisture, (**c**) precipitation, (**d**) vapor pressure deficit, (**e**) solar radiation, and (**f**) the most dominant factor. The bars on the left are the frequencies of the ridge regression coefficients between the EOS and the corresponding factors.

The partial correlation coefficients between the EOS and factors for different biome types are shown in Figure 6. The correlations between climatic factors and the EOS were obviously different among different biome types. In cases where the date of the EOS was postponed, the temperature was significant in most temperate grasslands, savannas, and shrublands (more than 70% of the pixels in the areas showed positive correlations). Precipitation was more important in temperate grasslands, savannas, and shrublands (positive in about 69%), and solar radiation was clearly more important in temperate broadleaf and mixed forests (positive in about 76%). VPD played a more vital role in deserts and xeric shrublands when compared with other factors (negative in about 68%), and the role of SM was the most dominant in montane grasslands and shrublands (positive in about 69%).

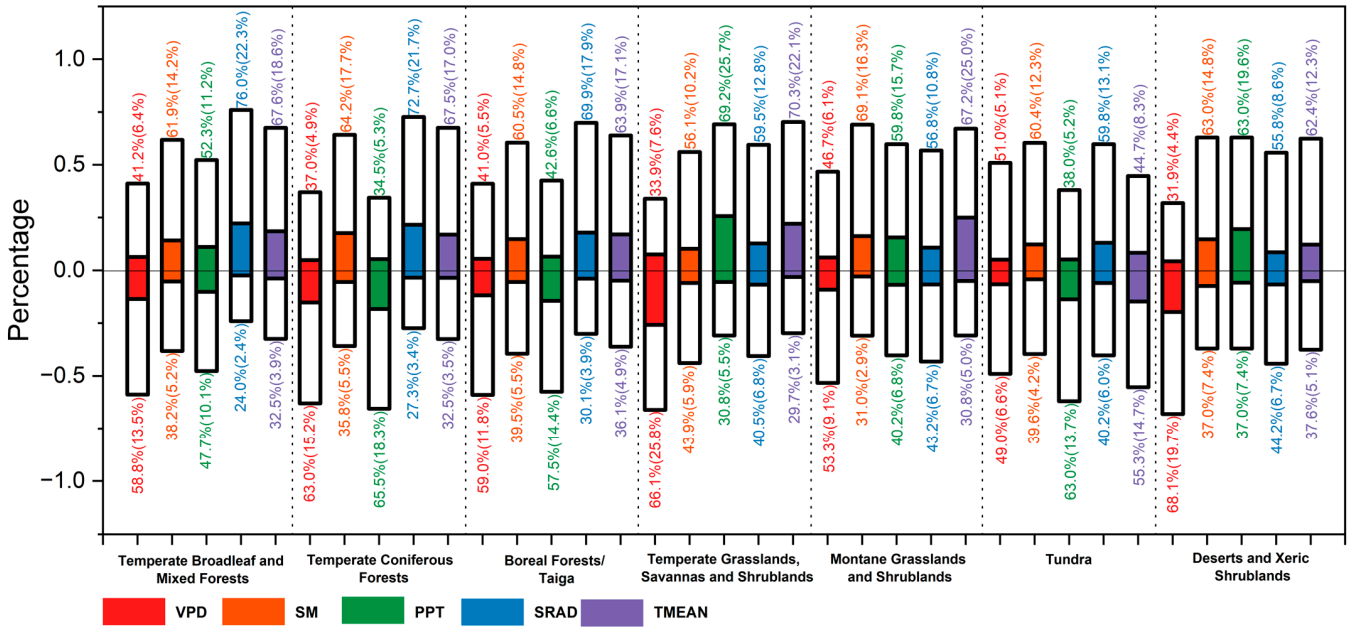

Figure 6. Partial correlation coefficients between the EOS and factors of each biome type. The bars above 0 represent percentages of positive correlations, and the others show negative percentages. Colored areas indicate significant percentages ($p < 0.05$).

The partial correlation coefficients between the EOS and factors for different climate zones are shown in Figure 7. The influences of climatic controls on the EOS were obviously different among climate zones. That the temperature postponed the date of the EOS was obvious in most BSk and Dfb (more than 68% of pixels in these climate zones showed positive correlations). Precipitation was more important in BSk (positive in about 74%); however, the effects of solar radiation were obvious in Dfb, Dfc, Dfd, Dwc, and ET (more than 59% of pixels in these climate zones showed positive correlations). VPD played a critical role in BSk and Dfb (more than 63% of pixels in these climate zones showed negative correlations). SM played a critical role in Cfb (positive in about 72%).

When coupling SM and VPD, it was hard to judge whether the advance in the EOS was due to low SM, high VPD, or both. However, regarding the variation in EOS across SM steps in the same VPD bins (the horizontal lines) and the transformation of EOS through VPD steps in the same SM bins (the vertical lines), the correlations between the EOS and SM or VPD without SM-VPD coupling are displayed in Figure 8.

The respective effects of SM and VPD on the EOS in the study area were examined and are shown in Figure 7. The variations in the EOS from low VPD to high VPD without SM-VPD coupling can quantify the VPD-induced stress on the EOS (the vertical lines). Meanwhile, variations in the EOS from high SM to low SM without SM-VPD coupling quantify SM-induced stress on the EOS (the horizontal lines). As the SM gradient decreased

and the VPD gradient increased, the EOS showed an advancing trend, and in the higher VPD bins and lower SM bins, the distribution of the EOS was less obvious.

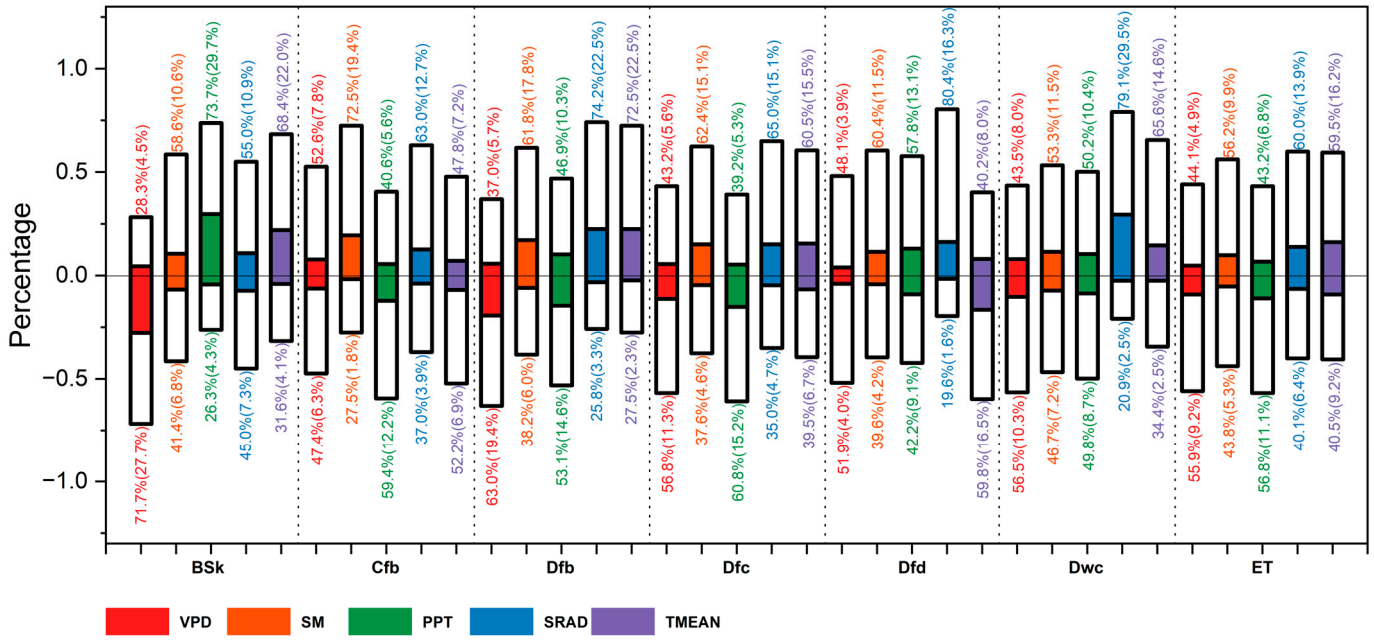

Figure 7. Partial correlation coefficients between the EOS and factors of each climate zone type. The bars above 0 represent percentages of positive correlations, and the others show negative percentages. Colored areas indicate significant percentages ($p < 0.05$).

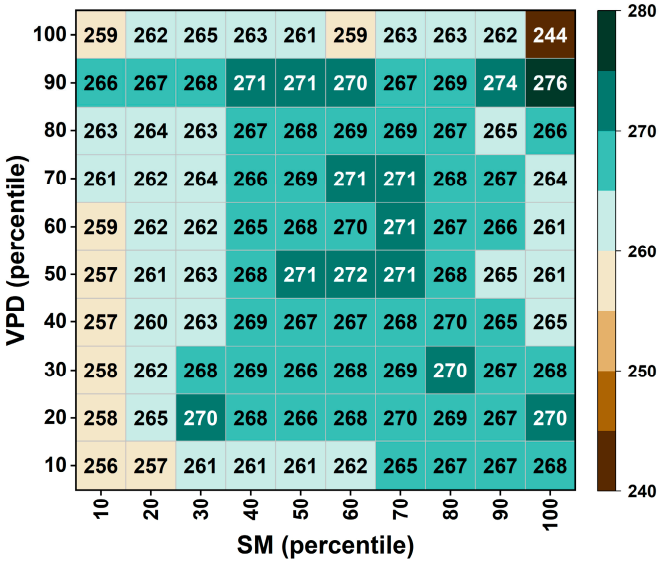

Figure 8. Average EOS in every percentile bin of SM and VPD.

As depicted in Figure 9, we investigated the partial correlation coefficients between the EOS and SM or VPD from 1982 to 2022. The mean coefficients between SM and EOS values rose at first and then fell above an LAI threshold (Figure 9a). The absolute value of the mean coefficients between VPD and EOS values rose at first and then fell above an LAI threshold (Figure 9b), which may indicate that vegetation with intermediate LAI values has a worse resistance to drought. The mean coefficients between SM and EOS values rose in most SM sections (Figure 9c), while the mean coefficients between VPD and EOS values declined in most VPD sections (Figure 9d), meaning that the effects of drought vary with the severity of drought.

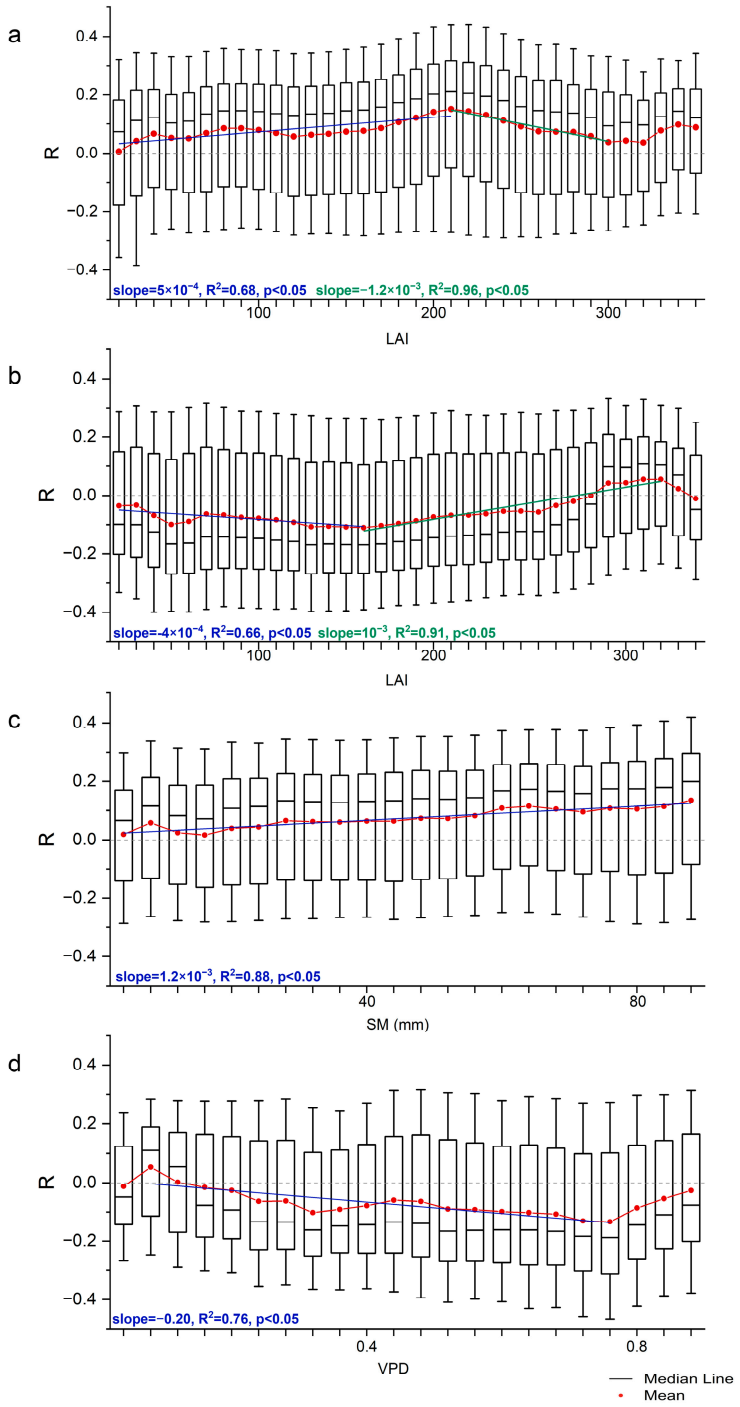

Figure 9. The correlations between the coefficients of partial correlation between EOS and SM (**a**,**c**), VPD (**b**,**d**), and the variables (LAI, LAI, SM, and VPD), respectively.

4. Discussion

4.1. The Trends of VPD, SM, and the EOS during the Period from 1982 to 2022

During the period from 1982 to 2022, VPD showed an increasing trend in most of the study area (Figure 3k), revealing the increasing trend of atmospheric drought. There was a trend of easing atmospheric drought in some regions in the north of the United States, the west of China, and northwestern Asia, which was a small percentage compared with the increasing trend. The significantly increasing values of VPD might have increased the sensitivity of the EOS to VPD, as shown in Figure 5d,f, and many studies have shown a

general trend of increasing atmospheric drought [18], revealing the impacts of deepening atmospheric drought on terrestrial vegetation [18,44].

In this period, the areas where SM showed an increasing trend and a decreasing trend were generally equal. The regions with increasing and decreasing trends of SM did not show a clear pattern (Figure 3g), which might lead to the conclusion that SM had a less significant effect on EOS than other factors in the experiment. At the same time, SM was affected by temperature increases, precipitation, NDVI, etc. [45], reflecting the interaction between climate factors, and by the interaction between the climate factors and terrestrial vegetation.

The EOS showed a postponing trend in most of the study area during the period, and an advancing trend was mainly found in high-latitude areas (Figure 3c). Some studies have shown that the EOS was mainly influenced by temperature and solar radiation with global warming [46–48].

Over time, drought has intensified at an increasing pace, which might become even more serious in the future as global warming intensifies. At the same time, more serious drought will deepen the impact on the growth of terrestrial vegetation [49,50]. Therefore, the long-term monitoring of VPD and SM is necessary for research on vegetation and the carbon sink, as well as government policy.

4.2. The Responses of the EOS to VPD and SM

SM can limit vegetation photosynthesis directly by determining the yield of water extracted by vegetation roots [22], affecting the EOS significantly and directly. We showed the effects of SM on the EOS and the sensitivity of the EOS to SM.

By contributing to the closing of stomata of vegetation and then reducing vegetation productivity, a high vapor pressure deficit could bring an earlier end to the growing season as well. However, some leaf-scale studies have shown that the stomatal conductance of some species (e.g., Douglas fir, Pseudotsuga menziesii, and Selaginella bryopteris) did not always decrease with increasing VPD [51,52]. In addition, as VPD increases, the evaporation rate increases and the nutrient uptake from the soil is enhanced [53,54], enhancing vegetation growth and possibly postponing the EOS. This phenomenon might show how vegetation responds and adapts to atmospheric dryness, and relevant studies might explain the positive correlations between the EOS and VPD. We found that there is a threshold LAI value that divides the influence of VPD and SM on vegetation phenology, and a threshold effect in response to VPD was proven in preceding studies [52,55,56].

Using a partial correlation analysis, we found that the impacts of VPD and SM on the EOS were almost equal to other factors and were thus not significantly more important. However, the EOS was markedly more sensitive to VPD than to other factors, which might be caused by the phenomenon in which vegetation adapts to atmospheric dryness, as mentioned above. Recent studies have also shown that the sensitivity of phenology to drought increased in the 21st century [57]. The regulatory mechanism of vegetation against atmospheric drought might play an important role in the process of resistance to atmospheric drought, which could reduce the impact of VPD on the EOS.

4.3. Responses Varied among Vegetation Types and Climate Zones

In this study, we found that the influences of VPD or SM on the EOS differed across various biome types and climate zones. VPD played a more important role in savannas, shrublands, temperate grasslands, deserts, and xeric shrublands. However, in tundra, the influence of VPD on the EOS was much weaker. In temperate coniferous forests, SM played a vital role; however, in temperate grasslands, savannas, and shrublands, the effect of SM on the EOS was small. At the climate level, VPD played a vital role in BSk and Dfb, but VPD played a very minor role in Dfd; SM was more significant in Cfb and Dfb, but the effect of SM on the EOS was smaller in ET.

Some studies showed that the effects of drought on vegetation in humid areas were less significant than in dry areas [58,59], and drought impacts were determined by water

stress levels and drought resistance among ecosystems, which were associated with water balance and vegetation characteristics [59].

In addition, in the areas more affected by drought, such as savannas, shrublands, and temperate grasslands, it was often more appropriate to consider the values of other influencing factors. The differences in the impacts of drought on the EOS could result from several causes, and more in-depth experiments are thus needed to explore the correlations between the EOS and drought.

4.4. Limitations

Our findings provided evidence for the roles of VPD and SM in terrestrial ecosystems and disentangled the interactions of VPD and SM in their effects on the EOS. Generally, an increasing VPD and decreasing SM may lead to an earlier EOS, while the effect VPD has on vegetation remains highly uncertain due to the complexity of and the many influences on vegetation phenology [60]. For example, in the literature, many previously unknown factors are increasingly being proven to impact the EOS. As many unproven factors were not considered in this analysis, the effects on the EOS as shown in the study might not be decided only by VPD and SM. In addition, the complex regulatory mechanisms of vegetation in response to adverse environments are not yet fully understood.

Because of the complex adaptation mechanisms of vegetation to dryness and the many factors affecting the EOS, there are still unknown effects of dryness on the EOS. At the same time, there are studies showing that drought can vary across different vegetation or areas and might change over time, and meteorological dryness and ecological responses can be so different that they are sometimes decoupled in time and space [61–63]. Continuous experiments will enhance our knowledge of the correlations between dryness and ecosystems.

5. Conclusions

Using remote sensing and meteorological data, our study provided a new understanding of the correlations between autumn vegetation phenology and dryness. It was found that the roles of VPD and SM were different in different climate zones and biome types: VPD contributed about 12.4% ($p < 0.05$) and SM contributed about 14.1% ($p < 0.05$) to an advanced EOS in the study area. Further comprehensive studies on the influences of drought on autumn vegetation phenology should therefore be conducted to obtain well-rounded conclusions.

Author Contributions: Conceptualization, X.W.; data curation, K.D.; methodology, K.D. and X.W.; writing—original draft, K.D.; writing—review and editing, X.W. All authors have read and agreed to the published version of the manuscript.

Funding: This work was funded by the National Natural Science Foundation of China (42271034) and the Youth Innovation Promotion Association of the Chinese Academy of Sciences (2022051).

Data Availability Statement: All data used in this study can be obtained openly. GIMMS3g+ can be obtained from https://daac.ornl.gov/VEGETATION/guides/Global_Veg_Greenness_GIMMS_3G.html, accessed on 10 September 2023. The Terraclimate dataset can be obtained from https://gee-community-catalog.org/projects/terraclim/, accessed on 15 September 2023.

Conflicts of Interest: The authors declare no conflicts of interest.

References

1. Humphrey, V.; Zscheischler, J.; Ciais, P.; Gudmundsson, L.; Sitch, S.; Seneviratne, S.I. Sensitivity of Atmospheric CO_2 Growth Rate to Observed Changes in Terrestrial Water Storage. *Nature* **2018**, *560*, 628–631. [CrossRef] [PubMed]
2. Piao, S.; Tan, J.; Chen, A.; Fu, Y.H.; Ciais, P.; Liu, Q.; Janssens, I.A.; Vicca, S.; Zeng, Z.; Jeong, S.J. Leaf Onset in the Northern Hemisphere Triggered by Daytime Temperature. *Nat. Commun.* **2015**, *6*, 6911. [CrossRef] [PubMed]
3. Wu, C.; Peng, D.; Soudani, K.; Siebicke, L.; Gough, C.M.; Arain, M.A.; Bohrer, G.; Lafleur, P.M.; Peichl, M.; Gonsamo, A. Land Surface Phenology Derived from Normalized Difference Vegetation Index (NDVI) at Global FLUXNET Sites. *Agric. For. Meteorol.* **2017**, *233*, 171–182. [CrossRef]

4. Fu, Y.H.; Zhao, H.; Piao, S.; Peaucelle, M.; Peng, S.; Zhou, G.; Ciais, P.; Huang, M.; Menzel, A.; Peñuelas, J. Declining Global Warming Effects on the Phenology of Spring Leaf Unfolding. *Nature* **2015**, *526*, 104–107. [CrossRef]
5. Estiarte, M.; Peñuelas, J. Alteration of the Phenology of Leaf Senescence and Fall in Winter Deciduous Species by Climate Change: Effects on Nutrient Proficiency. *Glob. Change Biol.* **2015**, *21*, 1005–1017. [CrossRef]
6. Richardson, A.D.; Keenan, T.F.; Migliavacca, M.; Ryu, Y.; Sonnentag, O.; Toomey, M. Climate Change, Phenology, and Phenological Control of Vegetation Feedbacks to the Climate System. *Agric. For. Meteorol.* **2013**, *169*, 156–173. [CrossRef]
7. Peng, J.; Wu, C.; Zhang, X.; Wang, X.; Gonsamo, A. Satellite Detection of Cumulative and Lagged Effects of Drought on Autumn Leaf Senescence over the Northern Hemisphere. *Glob. Change Biol.* **2019**, *25*, 2174–2188. [CrossRef]
8. Ahlström, A.; Raupach, M.R.; Schurgers, G.; Smith, B.; Arneth, A.; Jung, M.; Reichstein, M.; Canadell, J.G.; Friedlingstein, P.; Jain, A.K. The Dominant Role of Semi-Arid Ecosystems in the Trend and Variability of the Land CO_2 Sink. *Science* **2015**, *348*, 895–899. [CrossRef]
9. Reichstein, M.; Tenhunen, J.D.; Roupsard, O.; Ourcival, J.m.; Rambal, S.; Miglietta, F.; Peressotti, A.; Pecchiari, M.; Tirone, G.; Valentini, R. Severe Drought Effects on Ecosystem CO_2 and H_2O Fluxes at Three Mediterranean Evergreen Sites: Revision of Current Hypotheses? *Glob. Change Biol.* **2002**, *8*, 999–1017. [CrossRef]
10. Ge, W.; Han, J.; Zhang, D.; Wang, F. Divergent Impacts of Droughts on Vegetation Phenology and Productivity in the Yungui Plateau, Southwest China. *Ecol. Indic.* **2021**, *127*, 107743. [CrossRef]
11. Castillioni, K.; Newman, G.S.; Souza, L.; Iler, A.M. Effects of Drought on Grassland Phenology Depend on Functional Types. *New Phytol.* **2022**, *236*, 1558–1571. [CrossRef] [PubMed]
12. Allen, C.D.; Macalady, A.K.; Chenchouni, H.; Bachelet, D.; McDowell, N.; Vennetier, M.; Kitzberger, T.; Rigling, A.; Breshears, D.D.; Hogg, E.T. A global Overview of Drought and Heat-Induced Tree Mortality Reveals Emerging Climate Change Risks for Forests. *For. Ecol. Manag.* **2010**, *259*, 660–684. [CrossRef]
13. Madadgar, S.; AghaKouchak, A.; Farahmand, A.; Davis, S.J. Probabilistic Estimates of Drought Impacts on Agricultural Production. *Geophys. Res. Lett.* **2017**, *44*, 7799–7807. [CrossRef]
14. Cui, X.; Xu, G.; He, X.; Luo, D. Influences of Seasonal Soil Moisture and Temperature on Vegetation Phenology in the Qilian Mountains. *Remote Sens.* **2022**, *14*, 3645. [CrossRef]
15. Novick, K.A.; Ficklin, D.L.; Stoy, P.C.; Williams, C.A.; Bohrer, G.; Oishi, A.C.; Papuga, S.A.; Blanken, P.D.; Noormets, A.; Sulman, B.N. The Increasing Importance of Atmospheric Demand for Ecosystem Water and Carbon Fluxes. *Nat. Clim. Change* **2016**, *6*, 1023–1027. [CrossRef]
16. Sulman, B.N.; Roman, D.T.; Yi, K.; Wang, L.; Phillips, R.P.; Novick, K.A. High Atmospheric Demand for Water Can Limit Forest Carbon Uptake and Transpiration as Severely as Dry Soil. *Geophys. Res. Lett.* **2016**, *43*, 9686–9695. [CrossRef]
17. Novick, K.A.; Miniat, C.F.; Vose, J.M. Drought Limitations to Leaf-Level Gas Exchange: Results from a Model Linking Stomatal Optimization and Cohesion–Tension Theory. *Plant Cell Environ.* **2016**, *39*, 583–596. [CrossRef]
18. Yuan, W.; Zheng, Y.; Piao, S.; Ciais, P.; Lombardozzi, D.; Wang, Y.; Ryu, Y.; Chen, G.; Dong, W.; Hu, Z. Increased Atmospheric Vapor Pressure Deficit Reduces Global Vegetation Growth. *Sci. Adv.* **2019**, *5*, eaax1396. [CrossRef]
19. Yang, Y.; Yin, J.; Kang, S.; Slater, L.J.; Gu, X.; Volchak, A. Quantifying the Drivers of Terrestrial Drought and Water Stress Impacts on Carbon Uptake in China. *Agric. For. Meteorol.* **2024**, *344*, 109817. [CrossRef]
20. Zhong, Z.; He, B.; Wang, Y.-P.; Chen, H.W.; Chen, D.; Fu, Y.H.; Chen, Y.; Guo, L.; Deng, Y.; Huang, L. Disentangling the Effects of Vapor Pressure Deficit on Northern Terrestrial Vegetation Productivity. *Sci. Adv.* **2023**, *9*, eadf3166. [CrossRef]
21. He, B.; Chen, C.; Lin, S.; Yuan, W.; Chen, H.W.; Chen, D.; Zhang, Y.; Guo, L.; Zhao, X.; Liu, X. Worldwide Impacts of Atmospheric Vapor Pressure Deficit on the Interannual Variability of Terrestrial Carbon Sinks. *Natl. Sci. Rev.* **2022**, *9*, 150. [CrossRef] [PubMed]
22. Liu, L.; Gudmundsson, L.; Hauser, M.; Qin, D.; Li, S.; Seneviratne, S.I. Soil Moisture Dominates Dryness Stress on Ecosystem Production Globally. *Nat. Commun.* **2020**, *11*, 4892. [CrossRef] [PubMed]
23. Liu, L.; Peng, S.; AghaKouchak, A.; Huang, Y.; Li, Y.; Qin, D.; Xie, A.; Li, S. Broad Consistency between Satellite and Vegetation Model Estimates of Net Primary Productivity across Global and Regional Scales. *J. Geophys. Res. Biogeosci.* **2018**, *123*, 3603–3616. [CrossRef]
24. Stocker, B.D.; Zscheischler, J.; Keenan, T.F.; Prentice, I.C.; Peñuelas, J.; Seneviratne, S.I. Quantifying Soil Moisture Impacts on Light Use Efficiency across Biomes. *New Phytol.* **2018**, *218*, 1430–1449. [CrossRef]
25. Oren, R.; Sperry, J.; Katul, G.; Pataki, D.; Ewers, B.; Phillips, N.; Schäfer, K. Survey and Synthesis of Intra- and Interspecific Variation in Stomatal Sensitivity to Vapour Pressure Deficit. *Plant Cell Environ.* **1999**, *22*, 1515–1526. [CrossRef]
26. Zhang, X.; Rademacher, T.; Liu, H.; Wang, L.; Manzanedo, R.D. Fading Regulation of Diurnal Temperature Ranges on Drought-Induced Growth Loss for Drought-Tolerant Tree Species. *Nat. Commun.* **2023**, *14*, 6916. [CrossRef]
27. Li, W.; Migliavacca, M.; Forkel, M.; Denissen, J.M.; Reichstein, M.; Yang, H.; Duveiller, G.; Weber, U.; Orth, R. Widespread Increasing Vegetation Sensitivity to Soil Moisture. *Nat. Commun.* **2022**, *13*, 3959. [CrossRef]
28. Bateni, S.; Entekhabi, D. Relative Efficiency of Land Surface Energy Balance Components. *Water Resour. Res.* **2012**, *48*, W04510. [CrossRef]
29. Lian, X.; Piao, S.; Li, L.Z.; Li, Y.; Huntingford, C.; Ciais, P.; Cescatti, A.; Janssens, I.A.; Peñuelas, J.; Buermann, W. Summer Soil Drying Exacerbated by Earlier Spring Greening of Northern Vegetation. *Sci. Adv.* **2020**, *6*, eaax0255. [CrossRef]

30. Zhou, S.; Williams, A.P.; Berg, A.M.; Cook, B.I.; Zhang, Y.; Hagemann, S.; Lorenz, R.; Seneviratne, S.I.; Gentine, P. Land–Atmosphere Feedbacks Exacerbate Concurrent Soil Drought and Atmospheric Aridity. *Proc. Natl. Acad. Sci. USA* **2019**, *116*, 18848–18853. [CrossRef]
31. Piao, S.; Fang, J.; Zhou, L.; Ciais, P.; Zhu, B. Variations in Satellite-Derived Phenology in China's Temperate Vegetation. *Glob. Change Biol.* **2006**, *12*, 672–685. [CrossRef]
32. Olson, D.M. Terrestrial Ecoregionsof the Worlds: A New Map of Life on Earth. *Bioscience* **2001**, *51*, 933938. [CrossRef]
33. Friedl, M.; Sulla-Menashe, D. *Mcd12q1 Modis/Terra+Aqua Land Cover Type Yearly L3 Global 500 m SIN Grid V006 [Data set]*; NASA EOSDIS Land Processes Distributed Active Archive Center: Sioux Falls, SD, USA, 2019. [CrossRef]
34. Shen, M.; Nan, J.; Peng, D.; Rao, Y.; Yan, H.; Yang, W.; Zhu, X.; Cao, R.; Chen, X.; Chen, J. Can Changes in Autumn Phenology Facilitate Earlier Green-Up Date of Northern Vegetation? *Agric. For. Meteorol.* **2020**, *291*, 108077. [CrossRef]
35. Shen, M.; Zhang, G.; Cong, N.; Wang, S.; Kong, W.; Piao, S. Increasing Altitudinal Gradient of Spring Vegetation Phenology during the Last Decade on the Qinghai–Tibetan Plateau. *Agric. For. Meteorol.* **2014**, *189*, 71–80. [CrossRef]
36. Dardel, C.; Kergoat, L.; Hiernaux, P.; Mougin, E.; Grippa, M.; Tucker, C. Re-Greening Sahel: 30 Years of Remote Sensing Data and Field Observations (Mali, Niger). *Remote Sens. Environ.* **2014**, *140*, 350–364. [CrossRef]
37. Zhang, G.; Zhang, Y.; Dong, J.; Xiao, X. Green-up dates in the Tibetan Plateau Have Continuously Advanced from 1982 to 2011. *Proc. Natl. Acad. Sci. USA* **2013**, *110*, 4309–4314. [CrossRef]
38. Elmore, A.J.; Guinn, S.M.; Minsley, B.J.; Richardson, A.D. Landscape Controls on the Timing of Spring, Autumn, and Growing Season Length in Mid-A Tlantic Forests. *Glob. Change Biol.* **2012**, *18*, 656–674. [CrossRef]
39. Abatzoglou, J.T.; Dobrowski, S.Z.; Parks, S.A.; Hegewisch, K.C. TerraClimate, a High-Resolution Global Dataset of Monthly Climate and Climatic Water Balance from 1958–2015. *Sci. Data* **2018**, *5*, 170191. [CrossRef]
40. Wu, C.; Wang, X.; Wang, H.; Ciais, P.; Peñuelas, J.; Myneni, R.B.; Desai, A.R.; Gough, C.M.; Gonsamo, A.; Black, A.T.; et al. Contrasting Responses of Autumn-Leaf Senescence to Daytime and Night-Time Warming. *Nat. Clim. Change* **2018**, *8*, 1092–1096. [CrossRef]
41. Hoerl, A.E.; Kennard, R.W. Ridge Regression: Biased Estimation for Nonorthogonal Problems. *Technometrics* **1970**, *12*, 55–67. [CrossRef]
42. Qi, G.; She, D.; Xia, J.; Song, J.; Jiao, W.; Li, J.; Liu, Z. Soil Moisture Plays an Increasingly Important Role Role in Constraining Vegetation Productivity in China over the Past Two Decades. *Agric. For. Meteorol.* **2024**, *356*, 110193. [CrossRef]
43. Tu, Y.; Wang, X.; Zhou, J.; Wang, X.; Jia, Z.; Ma, J.; Yao, W.; Zhang, X.; Sun, Z.; Luo, P. Atmospheric Water Demand Dominates Terrestrial Ecosystem Productivity in China. *Agric. For. Meteorol.* **2024**, *355*, 110151. [CrossRef]
44. López, J.; Way, D.A.; Sadok, W. Systemic Effects of Rising Atmospheric Vapor Pressure Deficit on Plant Physiology and Productivity. *Glob. Change Biol.* **2021**, *27*, 1704–1720. [CrossRef] [PubMed]
45. Deng, Y.; Wang, S.; Bai, X.; Luo, G.; Wu, L.; Cao, Y.; Li, H.; Li, C.; Yang, Y.; Hu, Z. Variation Trend of Global Soil Moisture and Its Cause Analysis. *Ecol. Indic.* **2020**, *110*, 105939. [CrossRef]
46. Fu, Y.H.; Piao, S.; Delpierre, N.; Hao, F.; Hänninen, H.; Liu, Y.; Sun, W.; Janssens, I.A.; Campioli, M. Larger Temperature Response of Autumn Leaf Senescence than Spring Leaf-Out Phenology. *Glob. Change Biol.* **2018**, *24*, 2159–2168. [CrossRef]
47. Lang, W.; Chen, X.; Qian, S.; Liu, G.; Piao, S. A New Process-Based Model for Predicting Autumn Phenology: How is Leaf Senescence Controlled by Photoperiod and Temperature Coupling? *Agric. For. Meteorol.* **2019**, *268*, 124–135. [CrossRef]
48. Liu, Q.; Fu, Y.; Zeng, Z.; Huang, M.; Li, X.; Piao, S. Temperature, Precipitation, and Insolation Effects on Autumn Vegetation Phenology in Temperate China. *Glob. Change Biol.* **2016**, *22*, 644–655. [CrossRef]
49. Gray, S.B.; Dermody, O.; Klein, S.P.; Locke, A.M.; Mcgrath, J.M.; Paul, R.E.; Rosenthal, D.M.; Ruiz-Vera, U.M.; Siebers, M.H.; Strellner, R. Intensifying Drought Eliminates the Expected Benefits of Elevated Carbon Dioxide for Soybean. *Nat. Plants* **2016**, *2*, 16132. [CrossRef]
50. Wada, Y.; Van Beek, L.P.; Wanders, N.; Bierkens, M.F. Human Water Consumption Intensifies Hydrological Drought Worldwide. *Environ. Res. Lett.* **2013**, *8*, 034036. [CrossRef]
51. Soni, D.K.; Ranjan, S.; Singh, R.; Khare, P.B.; Pathre, U.V.; Shirke, P.A. Photosynthetic Characteristics and the Response of Stomata to Environmental Determinants and ABA in Selaginella Bryopteris, a Resurrection Spike Moss Species. *Plant Sci.* **2012**, *191*, 43–52. [CrossRef]
52. Woodruff, D.; Meinzer, F.; McCulloh, K. Height-Related Trends in Stomatal Sensitivity to Leaf-to-Air Vapour Pressure Deficit in a Tall Conifer. *J. Exp. Bot.* **2010**, *61*, 203–210. [CrossRef] [PubMed]
53. Lihavainen, J.; Ahonen, V.; Keski-Saari, S.; Sõber, A.; Oksanen, E.; Keinänen, M. Low Vapor Pressure Deficit Reduces Glandular Trichome Density and Modifies the Chemical Composition of Cuticular Waxes in Silver Birch Leaves. *Tree Physiol.* **2017**, *37*, 1166–1181. [CrossRef] [PubMed]
54. Oksanen, E.; Lihavainen, J.; Keinänen, M.; Keski-Saari, S.; Kontunen-Soppela, S.; Sellin, A.; Sõber, A. Northern Forest Trees under Increasing Atmospheric Humidity. *Prog. Bot.* **2019**, *80*, 317–336.
55. Cernusak, L.A.; Goldsmith, G.R.; Arend, M.; Siegwolf, R.T. Effect of Vapor Pressure Deficit on Gas Exchange in Wild-Type and Abscisic Acid–Insensitive Plants. *Plant Physiol.* **2019**, *181*, 1573–1586. [CrossRef] [PubMed]
56. Li, J.; Li, X. Response of Stomatal Conductance of Two Tree Species to Vapor Pressure Deficit in Three Climate Zones. *J. Arid Land* **2014**, *6*, 771–781. [CrossRef]

57. Wang, Y.; Tian, D.; Xiao, J.; Li, X.; Niu, S. Increasing Drought Sensitivity of Plant Photosynthetic Phenology and Physiology. *Ecol. Indic.* **2024**, *166*, 112469. [CrossRef]
58. Liu, Y.; Zhou, R.; Wen, Z.; Khalifa, M.; Zheng, C.; Ren, H.; Zhang, Z.; Wang, Z. Assessing the Impacts of Drought on Net Primary Productivity of Global Land Biomes in Different Climate Zones. *Ecol. Indic.* **2021**, *130*, 108146. [CrossRef]
59. Xu, H.-j.; Wang, X.-p.; Zhao, C.-y.; Yang, X.-m. Diverse Responses of Vegetation Growth to Meteorological Drought across Climate Zones and Land Biomes in Northern China from 1981 to 2014. *Agric. For. Meteorol.* **2018**, *262*, 1–13. [CrossRef]
60. Marchin, R.M.; Salk, C.F.; Hoffmann, W.A.; Dunn, R.R. Temperature Alone Does not Explain Phenological Variation of Diverse Temperate Plants under Experimental Warming. *Glob. Change Biol.* **2015**, *21*, 3138–3151. [CrossRef]
61. Cui, J.; Chen, A.; Huntingford, C.; Piao, S. Integrating Ecosystem Water Demands into Drought Monitoring and Assessment under Climate Change. *Nat. Water* **2024**, *2*, 215–218. [CrossRef]
62. Miller, D.L.; Wolf, S.; Fisher, J.B.; Zaitchik, B.F.; Xiao, J.; Keenan, T.F. Increased Photosynthesis during Spring Drought in Energy-Limited Ecosystems. *Nat. Commun.* **2023**, *14*, 7828. [CrossRef]
63. Yang, H.; Munson, S.M.; Huntingford, C.; Carvalhais, N.; Knapp, A.K.; Li, X.; Peñuelas, J.; Zscheischler, J.; Chen, A. The Detection and Attribution of Extreme Reductions in Vegetation Growth across the Global Land Surface. *Glob. Change Biol.* **2023**, *29*, 2351–2362. [CrossRef]